

## **Osteoinductive recombinant silk fusion proteins for bone regeneration**

Nina Dinjaski<sup>1\*</sup>, Robyn Plowright<sup>2\*</sup>, Shun Zhou<sup>1</sup>, David J. Belton<sup>2</sup>, Carole C. Perry<sup>2\*\*</sup>, David L. Kaplan<sup>1\*\*</sup>

<sup>1</sup> Department of Biomedical Engineering, Tufts University, 4 Colby Street, Medford, Massachusetts, 02155, United States.

<sup>2</sup> Biomolecular and Materials Interface Research Group, Interdisciplinary Biomedical Research Centre, School of Science and Technology, Nottingham Trent University, Clifton Lane, Nottingham, UK NG11 8NS.

\*\* To whom correspondence should be addressed:

David L. Kaplan. E-mail [David.Kaplan@Tufts.edu](mailto:David.Kaplan@Tufts.edu); Tel. (+617) 626 3251; Fax (+617) 627 3231

Carole C. Perry. E-mail [carole.perry@ntu.ac.uk](mailto:carole.perry@ntu.ac.uk) , Tel. +44 115 84 86695

\* These authors contributed equally to this work.

## **The statement of significance**

Organic-inorganic interfaces are integral to biomaterial functions in many areas of repair and regeneration. Several protein polymers have been investigated for this purpose. Despite their success the limited options to fine-tune their material properties, degradation patterns and functionalize them for each specific biomedical application limits their application. Various studies have shown that the biological performance of such proteins can be improved by genetic engineering. The present study provides data relating protein design parameters and functional outcome quantified by biomineralization and human mesenchymal stem cell differentiation. As such, it helps the design of osteoinductive recombinant biomaterials for bone regeneration.

## **Abstract**

Protein polymers provide a unique opportunity for tunable designs of material systems due to the genetic basis of sequence control. To address the challenge of biomineralization interfaces with protein based materials, we genetically engineered spider silks to design organic-inorganic hybrid systems. The spider silk inspired domain (SGRGGLGGQG AGAAAAAGGA GQGGYGGLGSQGT)<sub>15</sub> served as an organic scaffold to control material stability and to allow multiple modes of processing, whereas the hydroxyapatite binding domain VTKHLNQISQSY (VTK), provided control over osteogenesis. The VTK domain was fused either to the N-, C- or both terminals of the spider silk domain to understand the effect of position on material properties and mineralization. The addition of the VTK domain to silk did not affect the physical properties of the silk recombinant constructs, but it had a critical role in the induction of biomineralization. When the VTK domain was placed on both the C- and N-termini the formation of crystalline hydroxyapatite was significantly increased. In addition, all of the recombinant proteins in film format supported the growth and proliferation of human mesenchymal stem cells (hMSCs). Importantly, the presence of the VTK domain enhanced osteoinductive properties

up to 3-fold compared to the control (silk alone without VTK). Therefore, silk-VTK fusion proteins have been shown suitable for mineralization and functionalization for specific biomedical applications.

Keywords: silk; spider silk; hydroxyapatite; fusion proteins; biomaterials; calcification

## 1. Introduction

Recombinant biomaterials hold potential for the development of application-specific fine-tuned scaffolding for tissue regeneration and replacement, a major health challenge worldwide [1]. Organic-inorganic interfaces are integral to biomaterial functions in many areas of repair and regeneration, therefore the surface modification of implantable biomaterial surfaces with bioactive peptides is one approach to design materials for bone formation [2,3]. Several fibrous proteins have been investigated for this purpose [4,5]. Collagens are of particular interest as scaffolds for bone tissue engineering as they represent the major protein fraction of bone extracellular matrix [6]. However, collagen-based biomaterials generally lack mechanical stability and lose integrity over time [7]. Another unique family of fibrous proteins with impressive mechanical properties, biocompatibility and biodegradability are silks [8–12]. The mechanical properties of spider silk exceed other natural polymers and most synthetic materials, rivalling even high-performance fibers such as Kevlar, making silk a suitable candidate for bone-related biomaterials [13].

Biomimetic inorganic-organic hybrid systems have been analyzed as a route to stiffer and stronger materials [14–17]. To enhance osseointegration, silk has been specifically functionalized with different biological molecules [15–18]. Nevertheless, there is limited data on how these functional domains influence the material properties of silk [16]. Previously, silk-silica peptide designs were generated with studies focusing on understanding the role of the biomineralization domain position relative to the silk component in the silk-silica fusion proteins in terms of silica formation *in vitro* [16]. The silica-binding peptide R5 (SSKSGSYSGSKGSKRRIL) taken from the silaffin gene of *Cerithiopsis fusiformis* was fused to the N- or C-terminus of the silk sequence (SGRGGLGGQGAGAAAAGGAGQGGYGGLGSQGT)<sub>15</sub>, derived from the consensus repeat of *Nephila clavipes* dragline silk protein [16]. These fusion proteins were around 43 kDa. Herein, we designed silk based biomaterials to induce hydroxyapatite formation and enhance *in vitro* bone regeneration. Hydroxyapatite was selected as the target inorganic material due to its importance in bone tissues [19].

Optimal peptide candidates for bone regeneration have been identified *via* phage display, with VTKHLNQLSQSY (VTK) as a candidate with preferential interactions with both bone-like minerals and hydroxyapatite [20,21]. Since, the VTK peptide alone does not possess adequate mechanical properties for bone graft engineering, combination with appropriate scaffolding material is required.

In this study, we genetically modify the artificial silk polymer, 15mer ((SGRGGLGGQGAGAAAAAGGAGQGGYGGLGSQGT)<sub>15</sub>, ~ 39 kDa), derived from the consensus repeat of *N. clavipes* dragline silk protein with the hydroxyapatite binding peptide VTK, with the aim to build a biomaterial with potential application in bone grafting, exploiting both the remarkable mechanical properties of silk and the biomineralization properties of the VTK peptide. To identify optimal protein design with regard to mechanical performance and osteoinductive properties, the VTK peptide was fused separately to the N-, C- or both termini of the spider silk. The influence of the designs on calcium phosphate deposition with respect to crystallinity was assessed *in vitro*, along with the impact on beta sheet content as a proxy for mechanical strength. These assessments provide insight into structure-function relationships and the effect of functional domains on silk secondary structure/folding and functionalization for bone regeneration.

## **2. Materials and Methods**

### *2.1. Construction of recombinant silk and silk-VTK chimeras*

The following constructs were designed: 15mer-ch, nh-15mer, VTK-15mer-ch, nh-15mer-VTK and VTK-15mer-VTK (Fig. 1). The 15mer-ch and nh-15mer are spider silk constructs built of 15 repeating units (SGRGGLGGQG AGAAAAAGGA GQGGYGGLGSQGT)<sub>15</sub> that carry a Histidine tag (His<sub>6</sub> = h) on the C-terminal and N-terminal, respectively. VTK-15mer-ch is a 15mer-ch construct that has the VTK sequence (VTKHLNQLSQSY) [20,21], at the N-terminus, whereas nh-15mer-VTK is a nh-15mer that has the VTK sequence at the C-terminus. Plasmids pET30ch and pET30nh were used as cloning vectors, where the His-tag was located at the C- or N-termini of the genetic constructs, respectively. Both pET-30ch and pET-30nh are pET-30a(+) (Novagen, San Diego, CA, USA) derivative vectors. The construction

of the cloning vectors pET-30ch and pET-30nh was performed as described previously [16]. Next, a 1485bp DNA *NheI/SpeI* fragment containing genetic sequence coding for the artificial silk protein, 15mer (SGRGGLGGQGAGAAAAAGGAGQGGYGGLGSQGT)<sub>15</sub>, was inserted into pET30ch and pET30nh to yield pET30ch-15mer and pET30nh-15mer, respectively. To prepare the chimeras with the VTK sequence fused at the C-, N- or both termini of the 15mer, pET30ch-15mer and pET30nh-15mer were digested with *SpeI* and then treated with antarctic phosphatase (NEB, Ipswich, MA, USA) to prevent self-ligation. The nucleotide sequences of VTK were designed with restriction endonuclease sites *NheI* and *SpeI* flanked at the 5' and 3' termini, respectively. Codons were optimized for expression in *Escherichia coli* strain BL21(DE3) using the on-line tool OPTIMIZER and were synthesized commercially (Invitrogen, Grand Island, NY, USA). The synthesized nucleotides were annealed to generate double strands and then ligated to generate the constructs pET30ch-VTK-15mer, pET30nh-15mer-VTK and pET30-VTK-15mer-VTK. *E. coli* DH5 $\alpha$  cells were transformed and positive clones were selected with Luria Bertani (LB) (Sigma-Aldrich, St. Louis, MO, USA) plates supplemented with kanamycin (50  $\mu$ g/mL) (Sigma-Aldrich, St. Louis, MO, USA).

## 2.2. Expression and purification of recombinant silk and silk-VTK chimeras

The recombinant silk constructs were expressed in *E. coli* strain BL21 Star (DE3) (Invitrogen, Grand Island, NY, USA). A fermentor (Bioflo 3000, New Brunswick Scientific, Edison, NJ, USA) was used for the expression. Cells were cultivated at 37°C in LB medium with 50  $\mu$ g/mL kanamycin. Once the optical density OD<sub>600</sub> reached 0.8, isopropyl  $\beta$ -d-1-thiogalactopyranoside, IPTG (Sigma-Aldrich, St. Louis, MO, USA) was added at a final concentration of 1 mM to induce expression. After 5 h cells were harvested by centrifugation for 20 min at 8,000 rpm. Recombinant silk protein and chimeras were purified by Ni-NTA affinity chromatography as previously described [22], while the VTK-15mer-VTK protein that lacked the His-tag was purified by heat/ammonium sulphate precipitation [23,24]. Once purified, the proteins were dialyzed and lyophilized [25]. Protein identity and purity were confirmed by SDS-PAGE (Invitrogen, Grand Island, NY, USA).

### *2.3. Solution Studies*

#### *2.3.1. Zeta Potential*

The charge of each protein sample was determined by zeta potential measurements (NanoS Zetasizer, Malvern, UK) over a pH range of 2 to 9. A solution of each recombinant protein was prepared at a concentration of 1 mg/mL in 0.1 M citric acid. The solutions were filtered using a 200 nm membrane and the pH was adjusted by the addition of 0.1 M bis tris propane buffer. Five measurements were collected at each pH and an average taken.

#### *2.3.2. Mineralization in aqueous media*

Aqueous recombinant silk solutions (1 mg/mL) were prepared using: nh-15mer, nh-15mer-VTK, 15mer-ch, VTK-15mer-ch and VTK-15mer-VTK. For induction of mineralization, 2 mL of 200 mM calcium chloride and 2 mL of 120 mM sodium phosphate were alternately added as 100  $\mu$ L aliquots to 1 mL of each recombinant protein solution. A pH of 7.4 was maintained using 1 M sodium hydroxide (Fisher Scientific, Loughborough, UK). The solutions were kept at 37°C for 1 hour before the precipitates were collected and washed using dd H<sub>2</sub>O.

#### *2.3.3. Precipitate characterization*

Powder x-ray diffraction XRD (PANalytical X'Pert PRO, Cu K $\alpha$  radiation with wavelength of 1.54056 Å) was used to characterize the crystallinity of the precipitates produced. Aluminium sample holders were used and packed with polydimethylsiloxane (PDMS) (Sylgard 184 PDMS, MIsolar, Campbell, CA, USA), samples were scanned from 5° to 65° of 2 $\theta$ , accelerating voltage 45 kV, filament current 40 mA and scanning speed 0.02° s<sup>-1</sup>. X'PertHighScore Plus (Version 2.0a) was used for pattern manipulation (baseline correcting and smoothing) and analysis.

### *2.4. Silk Films*

#### *2.4.1. Silk Film production*

The lyophilized recombinant fusion proteins (15mer-ch, nh-15mer, VTK-15mer-ch, nh-15mer-VTK, VTK-15mer-VTK) were prepared at a concentration of 2.5% (wt/vol) in ultrapure water. The proteins were allowed to dissolve overnight at 4°C. PDMS (Sylgard 184 PDMS, MIsolar, Campbell, CA, USA) disks (R=6 mm) were used as substrates on which 30 µL aliquots of each protein solution was deposited, ensuring full coverage of each disk. Films were air-dried overnight and subsequently subjected to water vapor annealing using an isotemp vacuum oven for 24 h at room temperature and –25 inHg (635 mbar). Afterwards, films were air-dried overnight at room temperature.

#### *2.4.2. Mineralization of recombinant silk and silk-VTK films*

For induction of chemical mineralization, the recombinant proteins (15mer-ch, nh-15mer, VTK-15mer-ch, nh-15mer-VTK, VTK-15mer-VTK) mounted on PDMS substrates, as well as PDMS disks with no protein film, were placed in 24 well plates with 10 mL of 1:1 solution of 12 mM NaH<sub>2</sub>PO<sub>4</sub> pH 7.4 (adjusted using NaOH) and 20 mM CaCl<sub>2</sub> (Sigma-Aldrich, Dorset, UK).[26] After incubation for seven days at room temperature, the films were rinsed twice with water to remove soluble salts and left to dry overnight. Data for mineralisation on the PDMS disks alone did not influence mineralization (data not shown).

#### *2.4.3. Scanning electron microscopy (SEM) and energy-dispersive X-ray spectroscopy (EDX)*

SEM-EDX at 20 kV (JEOL 840, UK with Oxford Instruments Inca X-ray microanalysis, Oxford, UK) was used to observe the morphology and size of deposits post mineralization of recombinant silk films. Elemental composition of the films was analysed. Each sample was mounted onto electrically conducting carbon tape on aluminium stubs before being gold coated using an argon gold plasma at 30 mV and 1.2 kV for 2 minutes.

#### *2.4.4. Wettability and surface energy measurements*

The wettability and surface energy of each sample was measured using a Theta Attension Instrument with OneAttention v 1.7 software (Biolin Scientific, Staffordshire, UK). A silk film mounted on a PDMS

substrate was placed on the stand, and using a syringe, a 10  $\mu\text{L}$  droplet of water, dimethyl formamide (DMF) or ethylene glycol was placed on the surface and the contact angle at each side of the droplet measured ten times and an average taken. It was not possible to measure contact angles of the non-annealed films with DMF and ethylene glycol as the proteins dissolved in the solvents.

#### *2.4.5. Fourier Transform Infrared Attenuated Total Reflectance Spectroscopy (FTIR-ATR)*

Protein conformation was assessed using FTIR-ATR (Frontier, PerkinElmer, Coventry, UK), with an average of 40 scans over the range 4000-650  $\text{cm}^{-1}$ . Silk films were analysed before and after annealing to observe changes in structure. Thermo Grams A1 software v8.0 was used for curve fitting (including peak deconvolution), including baseline corrections. Six points were chosen from the amide I band (1700-1580  $\text{cm}^{-1}$ ), and 4 for the conformer absorbances ( $\beta$ -turn 1690–1662  $\text{cm}^{-1}$ ,  $\alpha$ -helix 1662–1645  $\text{cm}^{-1}$ , random coil 1645–1637  $\text{cm}^{-1}$ ,  $\beta$ -sheet 1637–1613  $\text{cm}^{-1}$ ). Absorbance bands were restricted to these parameters with the width limited to between 8 and 30  $\text{cm}^{-1}$  (at half height). An iteration was carried out forcing all peaks to have a positive area with a linear baseline. This was carried out for 1,000 iterations before curve fitting. The sum of the areas under the peaks was found and each conformer expressed as a percentage of the total.

#### *2.5. Cell Survival, Proliferation and Osteogenesis*

Human mesenchymal stem cells (hMSCs) were separated from a single fresh bone marrow aspirate (Lonza, Basel, Switzerland), cultured in DMEM (Thermo Fisher Scientific, Boston, MA, USA) (supplemented with 10% fetal bovine serum, 0.1 mM non-essential amino acids, 1 ng/mL bFGF, 1% antibiotic/antimycotic) and seeded at passage 2, as previously described [27]. These cells were characterized by their ability to undergo chondrogenic and osteogenic differentiation [28]. To assess the potential of hMSC for osteogenic, chondrogenic and adipogenic differentiation, the cells were cultured in pellets in either control supplemented DMEM medium as stated before, or osteogenic medium (StemPro Osteogenesis Differentiation Kit, Gibco, Life Technologies, Grand Island, NY, USA), chondrogenic medium (StemPro Chondrogenesis Differentiation Kit, Gibco, Life Technologies, Grand

Island, NY, USA), or adipogenic medium (StemPro Adipogenesis Differentiation Kit, Gibco, Life Technologies, Grand Island, NY, USA). To analyse the formation of bone-, cartilage- and fat-like tissue, samples were stained with Alizarin Red S, Alcian Blue and Oil Red O, respectively [28].

For seeding, recombinant silk-VTK films were prepared as described above, sterilized in ethylene oxide for 16 h at 4°C [29] and stored aseptically until seeding. Cells were seeded at a density of 5,000 cells per cm<sup>2</sup>, and allowed to adhere for 30 min prior to flooding with media. All cell culture was performed in an incubator maintained at 37°C and 5% CO<sub>2</sub>. The cells were cultured in hMSC media until 85% confluency, and then the medium was changed to an osteogenic medium. The medium was changed every 3–4 days. Cell growth and shape were monitored using a phase-contrast light microscope (Carl Zeiss, Jena, Germany) equipped with a Sony Exwave HAD 3CCD (Sony Electronics Inc., Park Ridge, NJ, USA) colour video camera.

#### *2.5.1. Cell viability*

Cell adherence and viability were determined 3, 7 and 14 days post seeding, using LIVE/DEAD Viability/Cytotoxicity Kit (Life Technologies, Grand Island, NY, USA) following the protocol recommended by the manufacturer. Briefly, cells were incubated with calcein AM and ethidium homodimer-1 (EthD-1) for 60 min to stain live (green) and dead cells (red), respectively. After staining, the films were washed three times with Phosphate Buffered Saline (PBS) and imaged using a fluorescence microscope (Keyence BZ-X700, Itasca, IL, USA) with excitation at 488 nm and emission at 499–537 nm for live cells and excitation at 543 nm and emission at 620–650 nm for dead cells.

#### *2.5.2. Metabolic activity*

The relative metabolic activity of the cells on each recombinant protein film before and after calcification (see Section 2.4) was determined by Alamar Blue assay (Life Technologies, Grand Island, NY, USA) according to the manufacturer's directions. Briefly, 2 weeks post seeding films were rinsed with PBS and incubated in DMEM medium with 10% Alamar Blue reagent for 4 h at 37°C with 5% CO<sub>2</sub>. Following incubation with the reagent, aliquots (100 µL) were placed into black 96 well plates and the

fluorescence quantified using a plate reader with an excitation wavelength of 550 nm and an emission wavelength of 590 nm. Cells plated in tissue culture wells were maintained as above and utilized as controls, while acellular films were used to adjust for background fluorescence.

### *2.5.3. Biochemical analysis of cellular calcification*

Eight weeks post-seeding, films were washed in PBS and osteogenesis was analysed by staining each film with Alizarin Red S (Sigma-Aldrich, St. Louis, MO, USA) to monitor calcium levels in deposits formed. Cells were fixed with 4% glutaraldehyde for 15 min and washed three times with PBS. Next, films were incubated with 2% Alizarin Red S pH 4.2 at room temperature in the dark for 30 min and washed 3 times with PBS. Calcification was monitored using a phase-contrast light microscope (Carl Zeiss, Jena, Germany) equipped with a Sony Exwave HAD 3CCD (Sony Electronics Inc., Park Ridge, NJ, USA) colour video camera. For quantitative analysis of calcium deposition, cells after 8 weeks of culture were first lysed in 0.2% (w/v) Triton X-100 and DNA content was measured using the PicoGreen assay (Molecular Probes, Eugene, OR, USA), according to the protocol of the manufacturer. Samples were measured fluorometrically at an excitation wavelength of 480 nm and an emission wavelength of 528 nm. "Calcium" was extracted twice with 0.5 mL 5% trichloroacetic acid. Calcium content was determined by a colorimetric assay using o-cresolphthalein complexone (Sigma Aldrich, St. Louis, MO, USA). The calcium complex was measured spectrophotometrically at 575 nm.

### *2.5.4. Immunostaining of bone-sialoprotein*

hMSC cultures on recombinant silk protein films were fixed with 4% paraformaldehyde and permeabilized with PBS containing 0.1% Triton X-100. Cells were incubated at 4°C overnight in a 1:300 dilution of the rabbit (IgG) polyclonal antibody against human bone sialoprotein in PBS containing 2 mg/mL of bovine serum albumin (BSA). The films were washed with ice-cold PBS for 10 min at room temperature and incubated for 1 h at room temperature with goat-anti-rabbit immunoglobulin secondary antibodies conjugated with FITC (Sigma Chemical, St. Louis, MO, USA), diluted 1:50 in PBS. Next, the films were rinsed with PBS plus 0.01% Triton X-20 and placed on coverslips. Immunostaining

was visualized by fluorescent microscopy (Keyence BZ-X700, Itasca, IL, USA) with excitation at 488 nm and emission at 499–537 nm.

### *2.6. Statistical Analysis*

All data provided are taken from averages with the total number of data points denoted by  $N=x$  and the error plotted as a function of standard deviation. The protein conformation data is based on 3 separate measurements on different samples, all zeta potential measurements were repeated 5 times and contact angle measurements were performed 20 times, 10 at each of the left and right contact angle. Biochemical parameters of cell viability and osteogenic differentiation were evaluated by Student's t-test. Differences between groups of  $p \leq 0.05$  were considered statistically significant. All quantitative data are presented as means  $\pm$  standard deviation.

## **3. Results**

### *3.1. Recombinant silk fusion protein design and production*

Recombinant silk fusion proteins were designed by fusing the hydroxyapatite-binding peptide VTK to the N-, C- or both termini of the artificial silk 15mer, derived from the consensus repeat of *N. clavipes* dragline silk protein. The addition of VTK domains to a spider silk resulted in recombinant silk fusion constructs with new functions for biomineralization. The silk domain contributes to the formation of  $\beta$ -sheet structures leading to crystallinity as a proxy for mechanical strength, while the VTK domain facilitates the biomineralization. Peptide design was focused on understanding the role of the hydroxyapatite binding domain position relative to the silk component in fusion proteins in terms of protein folding and biomineralization. With that aim, a set of fusion proteins, nh-15mer (40 kDa), 15mer-ch (40 kDa), nh-15mer-VTK (42 kDa), VTK-15mer-ch (42 kDa) and VTK-15mer-VTK (43 kDa), was designed (Fig. 1A). Figure 1B shows the successful expression and purification of these recombinant spider silk fusion proteins.

### *3.2. Solution Studies*

### 3.2.1. Protein charge in solution: zeta potential measurements

Stability in solution was determined *via* zeta potential measurements, where particles with a zeta potential -5 mV to 5 mV were considered highly unstable and prone to aggregation, those with a zeta potential more/less than  $\pm 30$  mV were considered to be stable [30]. In order to produce a stable colloidal system using the recombinant silk samples, the balance of surface charges of the dispersed phase has to be established to inhibit hydrophobic effects and aggregation of silk in solution. Therefore, to assess the optimal surface charge that resulted in isolated chains within a solution, the pH of the solution was varied. Figure 2B shows that all samples had non-stable particles between pH 5-7 with an isoelectric point between pH 5.5 and pH 6. However, under more acidic or more alkaline conditions (pH 3 and pH 9) all silk particles in solution could hold charge and increased in stability (Fig. 2B). The location of a single VTK peptide relative to the larger silk component had little effect on overall protein charge as assessed by zeta potential. However, constructs prepared with two VTK domains at either end of the polypeptide chain exhibited the lowest charge at ca. physiological pH.

### 3.2.2. Mineralization in solution

The effect of each recombinant silk construct on the formation of calcium phosphate from solution was explored (Fig. 2A), a constant pH of 7.4 was maintained throughout *via* addition of reagent in small aliquots as necessary. With no added protein, the material formed gives a dominant peak at ca.  $11.9^\circ$  signifying the presence of brushite ( $\text{CaHPO}_4 \cdot 2\text{H}_2\text{O}$ ) crystals [31]. Addition of the nh-15mer and 15mer-ch control proteins (no VTK domain) appeared to have no effect on the precipitates formed, whilst addition of the nh-15mer-VTK and VTK-15mer-ch proteins had similar but limited effects on the precipitates formed producing a mixture of calcium phosphates (predominantly hydroxyapatite and brushite) (Fig. 2A). The location of the VTK peptide in relation to the silk component did affect the relative proportions of each of the mineral phases formed with increased HAP being formed when the VTK peptide was located on the C terminus of the silk. In contrast, mineralization in the presence of VTK-15mer-VTK construct produced hydroxyapatite (HAP) alone, albeit the positions of peaks in the

X-ray diffraction pattern suggested the presence of a mineral phase with defects (Fig. 2A) [32–34]. The absence of a peak at approximately  $11.9^\circ$  arising from brushite, for materials prepared in the presence of the VTK-15mer-VTK protein indicated that significant changes in the mechanism of precipitation had occurred which were not observed for the other silk-based constructs used in the study (Fig. 2A). These results suggested that either there was a minimum VTK peptide concentration required to induce HAP formation or that the presence of the His tag hindered the formation of the apatite materials. To investigate this, mineralization in the presence of varying concentrations of the VTK-15mer-VTK protein construct were performed (Fig. 3). At the lowest protein concentrations used both brushite and HAP were identified with the contribution from brushite disappearing at protein concentration was increased to 1 mg/mL and above. A small shift of the peaks arising from the (002) and (004) planes to lower values of  $2\theta$  was observed as the level of protein used in the precipitation experiments was increased suggesting greater control over crystal growth in the z plane of the crystal structure versus the x and y planes.

Infra-red (FTIR) spectroscopy was used to compare precipitates formed in the presence of the various recombinant proteins. FTIR data (spectra shown in the SI), provide further evidence for the formation of phosphates in the presence of the silk based proteins, supporting the XRD data. There was no evidence of the presence of other organic material such as silk admixed in with the sample material though this might have been due to the limits of detection of the technique.

### 3.3. Silk Films

#### 3.3.1. *In vitro* hydroxyapatite mineralization on silk fusion proteins

Controlled mineralization was induced by incubation of the recombinant silk fusion proteins with solutions of  $\text{CaCl}_2$  and  $\text{NaHPO}_4$ . The potential for the different constructs to induce mineralization as annealed films *in vitro* was assessed by XRD, SEM and EDX.

Figure 4A shows XRD data for the precipitates formed on each silk film. All samples containing the VTK peptide; nh-15mer-VTK, VTK-15mer-ch and VTK-15mer-VTK, induced the formation of HAP as shown

by the broad peak at ca.  $32^\circ 2\theta$ , while mineralisation in the presence of films prepared from the constructs without the VTK peptide (nh-15mer and 15mer-ch) did not generate crystalline calcium phosphates. The position of the VTK peptide in relation to the silk construct did show an effect. When bound to the C terminal of the silk, the VTK domain had a greater ability to induce hydroxyapatite formation and, as for the mineralisation studies using the protein in solution, films made from the VTK-15mer-VTK silk construct were better still. FTIR data of the precipitates confirmed the presence of phosphates for the nh-15mer-VTK, VTK-15mer-ch and VTK-15mer-VTK films (Fig. 3B, phosphate peaks:  $550\text{ cm}^{-1} \nu_4(\text{PO}_4^{3-})$ ,  $960\text{ cm}^{-1} \nu_2(\text{PO}_4^{3-})$ ,  $1010\text{ cm}^{-1} \nu_3(\text{PO}_4^{3-})$ ) and with mixtures of phosphates and carbonates being observed for the control samples nh-15mer and 15mer-ch (carbonate peaks:  $850\text{ cm}^{-1} \nu_2(\text{CO}_3^{2-})$ ,  $1530\text{ cm}^{-1} \nu_3(\text{CO}_3^{2-})$ ). These results suggest that the VTK containing constructs are still able to direct mineralization when present as part of a solid construct.

SEM images coupled with EDX of the recombinant silk films post mineralization (Fig. 4C-G) again provide evidence for Ca/P mineralisation on the nh-15mer-VTK, ch-15mer-VTK and VTK-15mer-VTK films. Traces of sodium chloride were present on all analysed films arising from the solutions used in the mineralisation studies. The nh-15mer control sample showed minimal salt deposition, likely sodium chloride, whilst the 15mer-ch film promoted substantial deposition of a mixture of precipitates, containing calcium, chlorine and phosphorous.

### *3.3.2. Materials properties of the films*

The secondary structure of recombinant protein films (nh-15mer, nh-15mer-VTK, 15mer-ch, VTK-15mer-ch, VTK-15mer-VTK) was analysed by FTIR-ATR. The quantification of protein secondary structure was performed by peak deconvolution analysis of the amide I band. The position and shape of the amide I band changed with varying beta sheet content, as the C=O stretching vibrations are influenced by alterations to the conformation of the backbone of the structure and the pattern of hydrogen bonding present [35,36]. Figure 5 shows the changes in structural conformation of the silk films before and after annealing. Before annealing the control and VTK containing samples exhibited

similar percentages of beta sheet with the exception of the nh-15mer control sample, which contained more beta sheet initially, but showed the smallest structural transformation upon annealing. All samples were susceptible to induced beta structure formation, suggesting these samples have the potential to be tailored in terms of their physical properties. These changes were seen in the shift of the amide I band from  $1650\text{ cm}^{-1}$  to  $1630\text{ cm}^{-1}$ . Example deconvoluted spectra are shown in SI Fig. 2.

The wettability and surface energetics of the films was assessed by contact angle measurements on the silk films before and after water annealing. Surface energy calculations were only possible for the annealed films as the non-annealed films were not stable. Each prepared silk film was hydrophilic becoming more hydrophobic after annealing. Non-annealed films produced from the VTK containing samples were more hydrophobic than the control samples, but exhibited less structural change upon annealing (Fig. 5). The presence of the VTK peptide at the N terminus of the silk resulted in no significant change in surface energy, in direct contrast to the addition of the VTK domain at the C-terminus of the silk which resulted in a significant decrease in surface energy (from approx.  $30\text{ Jm}^{-2}$  to  $23\text{ Jm}^{-2}$ ).

#### *3.4. Cytocompatibility of chimeric silk-silica films and osteogenic potential*

To evaluate the potential of the recombinant silk fusion proteins to support cell growth and induce osteogenesis, human mesenchymal stem cells (hMSCs) were cultured on the surface of each film. Initially, hMSCs were isolated and their potential for osteogenic, chondrogenic and adipogenic differentiation were analysed. Preformed screens indicated that the isolated hMSCs had the potential for osteogenic, chondrogenic and adipogenic differentiation and thus represented suitable cells for further analysis of the recombinant silk fusion protein films (SI Fig. 3).

To analyse the ability of the silk fusion proteins to support hMSC growth and promote differentiation, the cells were grown on the various film surfaces and assessed by live/dead staining. Fluorescent imaging of live/dead staining confirmed that the hMSCs seeded on the mineralized films adhered to the surfaces when compared to control tissue culture plate (TCP) surfaces, and the mineralized films

also supported cell growth and proliferation for 2 weeks (Fig. 6A, SI Fig. 4). An elongated morphology of hMSCs was observed on all tested surfaces after 14 days suggesting healthy growth of hMSCs and an absence of cytotoxicity to the recombinant silk-silica fusion proteins (Fig. 6A). No differences in cell viability were observed between the different recombinant constructs. Similarly, non-biomineralized silk films supported hMSCs growth and proliferation (data not shown). An Alamar blue assay 2 weeks following seeding indicated good cell viability and metabolic activity of hMSCs grown on recombinant silk and silk-VTK constructs (Fig. 6B). Subsequently, these results showed that all analyzed pre-calcified and non-precalcified films supported cell adhesion, growth and proliferation.

To verify that the silk-VTK fusion protein films were able to enhance bone formation *in vitro*, hMSCs were cultured on the surface of the films. Osteogenic parameters were evaluated in the hMSC cultures grown on nh-15mer, nh-15mer-VTK, 15mer-ch, VTK-15mer-ch and VTK-15mer-VTK films, 8 weeks post seeding. The ability of films to enhance bone sialoprotein production and calcium deposition was assessed. The differences between bone sialoprotein deposition on nh-15mer, nh-15mer-VTK, 15mer-ch, VTK-15mer-ch, VTK-15mer-VTK and TCP were evaluated. A higher bone sialoprotein production was observed on the samples that carried the VTK domain (nh-15mer-VTK, VTK-15mer-ch, VTK-15mer-VTK) in comparison to the nh-15mer and 15mer-ch silk samples (Fig. 7A). Importantly, the highest amount of deposited bone sialoprotein was observed on VTK-15mer-VTK films (Fig. 7A). Analysis of calcium deposition supported this finding. Alizarin Red staining demonstrated the lower potential of the recombinant constructs lacking hydroxyapatite binding domain to induce osteogenesis when compared to the VTK constructs (Fig. 7B). Both the N- and C-terminal domain located VTK constructs promoted calcium deposition, however, the highest calcium deposition was observed on the VTK-15mer-VTK film, possibly due to the higher rate of calcification on these films. Control samples, 15mer-ch and nh-15mer, induced less calcium deposition, showing the importance of the VTK domain in the process. These results indicated that both position and number of VTK domains were important factors for the induction of *in vitro* osteogenesis. Quantitative analysis of calcium deposition showed 3-fold higher calcium deposition on the VTK-15mer-VTK construct when compared to silk alone (nh-

15mer, ch-15mer) (Fig. 7C). Furthermore, constructs carrying one VTK domain, nh-15mer-VTK and VTK-15mer-ch, showed lower potential to induce hMSC differentiation compared to VTK-15mer-VTK, demonstrated by lower calcium deposition induced by nh-15mer-VTK and VTK-15mer-ch ( $0.63 \pm 0.07$  and  $0.78 \pm 0.08$  Ca  $\mu\text{g}/\text{ng}$  total DNA), in comparison to VTK-15mer-VTK that induced the deposition of  $1.05 \pm 0.08$  Ca  $\mu\text{g}/\text{ng}$  total DNA ) (Fig. 7C).

#### **4. Discussion**

Advancements in tissue engineering and regenerative medicine are often dependent on the development of biocompatible and functional materials that can match the properties of target tissues. Genetically engineered biomaterials are useful for application specific functionalization owing to their rational design, tuneable structure-function features, biocompatibility, degradability and target specificity. Recombinant silk fusion proteins possess these properties. Additionally, given the benefits of combining semi-crystalline silk domains and hydroxyapatite binding domains, these proteins are promising candidates for tissue engineering and regenerative medicine, in particular for the field of bone regeneration. Mineral-binding sequences are rich in acidic residues (aspartate, glutamate, phosphoserines) and/or post-translational modifications resulting in a net negative charge that promotes binding to positively charged calcium at apatite crystal faces [20].

Some design parameters have been previously studied for silk-silica fusion proteins [15,16]. To understand mineralization interactions at different biomaterial interfaces able to modulate mineralization and efficiently define key parameters in material design, VTK constructs have been recombinantly produced and studied. These constructs have high relevance in human physiology due to their ability to induce hydroxyapatite formation. Previously, silicification studies from solution showed that the presence of the R5 domain induced silica particle deposition, and that the location of the R5 domain was critical for controlling the silicification process. Availability of target functional groups allowed the R5 peptide to have contact with silica in solution and therefore influence deposition at either terminus of the silk, but only when bound to the C-terminus was there restraint

over the size of silica particles produced [16]. Similarly, as reported in the present study, key parameters for the induction of biomineralization catalyzed by VTK functionalized silk in solution was the number of VTK domains alongside the position of the VTK domain (Scheme 1).

Addition of nh-15mer-VTK and VTK-15mer-ch chimeras to mineralization solutions resulted in a mixture of HAP and Brushite being formed. A comparison of the XRD patterns for materials generated in the presence of these two constructs suggested that the nh-15mer-VTK chimera was more effective at directing the formation of HAP as the intensities of the peaks arising from brushite in comparison to those arising from HAP were lower. When the VTK peptide was bound to the C-terminus of the silk, a larger density of hydroxyl groups are available for interaction with mineralizing ions, and this combined with a greater flexibility of the hydroxyl rich end of the peptide leads to a greater effect on mineralization. The opposite is true for VTK-15mer-ch, as the end of the VTK peptide with the greater density of hydroxyl groups is anchored to the silk domain, likely resulting in limited interactions with the reagents in solution and hence the peptide component is less able to affect the formation of mineralized precipitates (Scheme 1). When the same experiment was repeated using the VTK-15mer-VTK chimera, the precipitate formed was solely HAP, highlighting the fact that at either terminus the VTK peptide can be effective.

In addition, protein concentration was a critical factor to induce biomineralization. The protein concentration required to optimize physical properties to permit the VTK peptide to influence the formation of precipitates was defined using VTK-15mer-VTK construct. By increasing the concentration of the VTK-15mer-VTK protein the narrowing of the peaks in the XRD pattern was observed, suggesting an increase in crystallite size. Therefore, modification of protein concentration can be used to tailor the size of crystallites that form in the system. In addition, with increasing VTK-15mer-VTK concentration a significant shift in the XRD peaks with miller indices (002) and (004) towards apatite-like structure was observed, indicating that increased protein concentration leads to a reduction in homogenous strain in the z plane. This outcome is probably caused by the assembly of

the proteins into micelle-like structures, where the VTK domain is located on the outer surface of the micelle and is therefore more exposed to the solution. This effect is exhibited to a lesser extent with samples containing only one VTK domain, because as the proteins align to form the micelles there is a non-specific arrangement causing peripheral localization of some VTK domains and central localization of others. This results in the shielding of the VTK domains and exposure of the His-tag. This non-specific arrangement does not affect the VTK-15mer-VTK molecules due to either terminus holding the hydroxyapatite binding domain.

Silk materials possess high tensile strength due to the naturally occurring beta sheet features of the proteins when formed into fibers or other materials [37,38]. The percentage of beta conformers, both sheet and turn, are directly related to the physical properties exhibited by the silk, therefore it is important to measure and explore the ability to customise the beta content of such materials [24]. FTIR data showed an increase in beta conformers in all the recombinant films upon annealing, and this was supported by contact angle measurements with an increase in hydrophobicity and therefore beta content when films were annealed. The localization of the VTK domain in the silk-VTK fusion protein variants had no significant influence on the physical properties of the proteins. This data is in agreement with previously obtained results for the recombinant silk-R5 fusion proteins [16].

The chimeric protein samples carrying the VTK domain induced HAP formation. Similarly to what was found for solution based mineralization, the position and the number of hydroxyapatite binding VTK domains in the recombinant silk fusions had an impact on the level of mineralization on the film surfaces. The constructs harboring VTK domains on both the N- and C-termini induced the highest level of calcification when compared to all other constructs. This is possibly due to the difference in protein folding and exposure of the VTK domains that are the key factor in catalyzing the process. The effect of peptide location on mineralization (where the VTK domain being attached to the C terminal of silk allows easier access to a greater density of hydroxyl groups) was greater for the solid films than

the proteins in solution, probably due to hindered peptide motion restricting contact with mineralizing ions in the immediate environment of the film itself.

A central tenet of biomimetic material design for connective tissues is that replicating key aspects of biological tissues enables materials to achieve a greater level of control over cell functions, and allow better integration into host tissues [39]. Therefore, in addition to mentioned design parameters, both the composition and functional properties of a biomaterial influence cell adhesion, growth and subsequent differentiation. As demonstrated in the present study, all recombinant silk fusion protein films supported cell growth. The proliferation of the cells on the surface of silk-VTK films was not significantly different than on TCP. This result suggests that the recombinant silk fusion protein films were not cytotoxic.

The inherent complexity of skeletal and dental tissues requires not only that biomaterials elicit specific cellular responses that lead to extracellular matrix formation, but that the tissue formed is both spatially and temporally controlled, and can be mineralized [40]. While most biomaterials support cell growth and proliferation, mimicking the structure of calcified tissues and addressing the limitations of the individual materials in the development of organic-inorganic hybrid biomaterials provides excellent possibilities for improving conventional bone implants, as presented herein. Through combinatorial design we analysed the key parameters to control biomineralization on recombinant silk-VTK films and subsequently osteogenesis. We demonstrated that the VTK domain had the critical role in osteogenesis. As the VTK domain alone does not possess the required mechanical properties to support bone regeneration, the presence of silk 15mer played critical role in overall stability of the film. The construct harbouring VTK domains on both the N- and C-termini had the greatest impact in terms of the differentiation of hMSCs.

## **5. Conclusions**

These new recombinant silk-VTK proteins have been designed for potential utility in regenerative medicine. The manipulation of the fusion protein sequence allowed control of biomineralization. The

hydroxyapatite binding domain had a critical role in the induction of biomineralization. The location of the VTK peptide influenced the potential of the recombinant fusion protein variants to induce calcification. Nevertheless, the addition of the VTK domain to silk did not affect the physical properties of the silk recombinant constructs. Importantly, when the VTK domain was placed on both the C- and N-termini the formation of crystalline hydroxyapatite was significantly increased. All constructs supported proper cell growth and proliferation *in vitro* and the VTK-15mer-VTK construct had the highest potential to promote hMSC differentiation.

### **Acknowledgements**

We thank the NIH (R01 DE017207) for support of this work.

## References

- [1] U.S. Depart, H. Services, 2020 : A New Vision - A Future for Regenerative Medicine, (2010) 1–21.
- [2] H. Shin, S. Jo, A.G. Mikos, Biomimetic materials for tissue engineering, *Biomaterials*. 24 (2003) 4353–4364.
- [3] J. Hubbell, Bioactive biomaterials, *Curr. Opin. Biotechnol.* 10 (1999) 123–129.
- [4] M. Geiger, Collagen sponges for bone regeneration with rhBMP-2, *Adv. Drug Deliv. Rev.* 55 (2003) 1613–1629.
- [5] L. Meinel, R. Fajardo, S. Hofmann, R. Langer, J. Chen, B. Snyder, G. Vunjak-Novakovic, D. Kaplan, Silk implants for the healing of critical size bone defects., *Bone*. 37 (2005) 688–98.
- [6] A.H. Reddi, Morphogenetic messages are in the extracellular matrix: biotechnology from bench to bedside, *Biochem. Soc. Trans.* 28 (2000) 345–349.
- [7] J. Riesle, A.P. Hollander, R. Langer, L.E. Freed, G. Vunjak-Novakovic, Collagen in tissue-engineered cartilage: types, structure, and crosslinks., *J. Cell. Biochem.* 71 (1998) 313–27.
- [8] Y. Wang, U.-J. Kim, D.J. Blasioli, H.-J. Kim, D.L. Kaplan, In vitro cartilage tissue engineering with 3D porous aqueous-derived silk scaffolds and mesenchymal stem cells., *Biomaterials*. 26 (2005) 7082–94.
- [9] G.H. Altman, F. Diaz, C. Jakuba, T. Calabro, R.L. Horan, J. Chen, H. Lu, J. Richmond, D.L. Kaplan, Silk-based biomaterials, *Biomaterials*. 24 (2003) 401–416.
- [10] U.-J. Kim, J. Park, H.J. Kim, M. Wada, D.L. Kaplan, Three-dimensional aqueous-derived biomaterial scaffolds from silk fibroin., *Biomaterials*. 26 (2005) 2775–85.
- [11] B. Panilaitis, G.H. Altman, J. Chen, H.-J. Jin, V. Karageorgiou, D.L. Kaplan, Macrophage responses to silk, *Biomaterials*. 24 (2003) 3079–3085.

- [12] S. Sofia, M.B. McCarthy, G. Gronowicz, D.L. Kaplan, Functionalized silk-based biomaterials for bone formation., *J. Biomed. Mater. Res.* 54 (2001) 139–48.
- [13] T. Scheibel, Spider silks: recombinant synthesis, assembly, spinning, and engineering of synthetic proteins., *Microb. Cell Fact.* 3 (2004) 14.
- [14] S. Gomes, I.B. Leonor, J.F. Mano, R.L. Reis, D.L. Kaplan, Spider silk-bone sialoprotein fusion proteins for bone tissue engineering, *Soft Matter.* 7 (2011) 4964.
- [15] C. Wong, P. Foo, S. V Patwardhan, D.J. Belton, B. Kitchel, D. Anastasiades, J. Huang, R.R. Naik, C.C. Perry, D.L. Kaplan, Novel nanocomposites from spider silk – silica fusion ( chimeric ) proteins, *Proc. Natl. Acad. Sci.* 103 (2006) 9428–9433.
- [16] R. Plowright, N. Dinjaski, S. Zhou, D.J. Belton, D.L. Kaplan, C.C. Perry, Influence of silk-silica fusion protein designs on silica condensation in vitro and cellular calcification, *RSC Adv.* 6 (2016) 21776–21788.
- [17] J. Huang, C. Wong, A. George, D.L. Kaplan, The effect of genetically engineered spider silk-dentin matrix protein 1 chimeric protein on hydroxyapatite nucleation., *Biomaterials.* 28 (2007) 2358–67.
- [18] S. Gomes, I.B. Leonor, J.F. Mano, R.L. Reis, D.L. Kaplan, Natural and Genetically Engineered Proteins for Tissue Engineering, *Prog Polym Sci.* 37 (2013) 1–17.
- [19] B. Stevens, Y. Yang, A. Mohandas, B. Stucker, K.T. Nguyen, A review of materials, fabrication methods, and strategies used to enhance bone regeneration in engineered bone tissues, *J. Biomed. Mater. Res. Part B Appl. Biomater.* 85B (2008) 573–582.
- [20] W.N. Addison, S.J. Miller, J. Ramaswamy, A. Mansouri, D.H. Kohn, M.D. McKee, Phosphorylation-dependent mineral-type specificity for apatite-binding peptide sequences, *Biomaterials.* 31 (2010) 9422–9430.

- [21] S.J. Segvich, H.C. Smith, D.H. Kohn, The adsorption of preferential binding peptides to apatite-based materials, *Biomaterials*. 30 (2009) 1287–1298.
- [22] H. Dams-Kozłowska, A. Majer, P. Tomasiewicz, J. Lozinska, D.L. Kaplan, A. Mackiewicz, Purification and cytotoxicity of tag-free bioengineered spider silk proteins., *J. Biomed. Mater. Res. A*. 101 (2013) 456–64.
- [23] S.R. Fahnestock, S.L. Irwin, Synthetic spider dragline silk proteins and their production in *Escherichia coli*, *Appl. Microbiol. Biotechnol.* 47 (1997) 23–32.
- [24] D. Huemmerich, C.W. Helsen, S. Quedzuweit, J. Oschmann, R. Rudolph, T. Scheibel, Primary structure elements of spider dragline silks and their contribution to protein solubility., *Biochemistry*. 43 (2004) 13604–13612.
- [25] S. Zhou, W. Huang, D.J. Belton, L.O. Simmons, C.C. Perry, X. Wang, D.L. Kaplan, Control of silicification by genetically engineered fusion proteins: silk-silica binding peptides., *Acta Biomater.* 15 (2015) 173–80.
- [26] T. Tsuji, K. Onuma, A. Yamamoto, M. Iijima, K. Shiba, Physicochemical properties of artificial proteins that accelerate nucleation of crystalline calcium phosphate, *J. Cryst. Growth*. 314 (2011) 190–195.
- [27] G.H. Altman, R.L. Horan, H.H. Lu, J. Moreau, I. Martin, J.C. Richmond, D.L. Kaplan, Silk matrix for tissue engineered anterior cruciate ligaments., *Biomaterials*. 23 (2002) 4131–41.
- [28] L. Meinel, V. Karageorgiou, S. Hofmann, R. Fajardo, B. Snyder, C. Li, L. Zichner, R. Langer, G. Vunjak-Novakovic, D.L. Kaplan, Engineering bone-like tissue in vitro using human bone marrow stem cells and silk scaffolds., *J. Biomed. Mater. Res. A*. 71 (2004) 25–34.
- [29] J.R. Mauney, J. Blumberg, M. Pirun, V. Volloch, G. Vunjak-Novakovic, D.L. Kaplan, Osteogenic differentiation of human bone marrow stromal cells on partially demineralized bone scaffolds in vitro., *Tissue Eng.* 10 (2004) 81–92.

- [30] D.J. Belton, A.J. Mieszawska, H.A. Currie, D.L. Kaplan, C.C. Perry, Silk-silica composites from genetically engineered chimeric proteins: materials properties correlate with silica condensation rate and colloidal stability of the proteins in aqueous solution., *Langmuir*. 28 (2012) 4373–81.
- [31] G. Walsh, *Proteins: Biochemistry and Biotechnology*, 2002.
- [32] D.S. Bocciarelli, Morphology of crystallites in bone, *Calcif. Tissue Res.* 5 (1970) 261–269.
- [33] H.H. Roseberry, A.B. Hastings, J.K. Morse, X-ray analysis of bone and teeth, *J. Biol. Chem.* 90 (1931) 395–407.
- [34] D. Carlström, J.B. Finean, X-ray diffraction studies on the ultrastructure of bone, *Biochim. Biophys. Acta.* 13 (1954) 183–191.
- [35] J.L.R. Arrondo, A. Muga, J. Castresana, F.M. Goñi, Quantitative studies of the structure of proteins in solution by fourier-transform infrared spectroscopy, *Prog. Biophys. Mol. Biol.* 59 (1993) 23–56.
- [36] J.L.R. Arrondo, F.M. Goñi, Structure and dynamics of membrane proteins as studied by infrared spectroscopy, *Prog. Biophys. Mol. Biol.* 72 (1999) 367–405.
- [37] C. Fu, Z. Shao, V. Fritz, Animal silks: their structures, properties and artificial production., *Chem. Commun. (Camb)*. (2009) 6515–29.
- [38] O. Hakimi, D.P. Knight, F. Vollrath, P. Vadgama, Spider and mulberry silkworm silks as compatible biomaterials, *Compos. Part B Eng.* 38 (2007) 324–337.
- [39] D. Green, D. Walsh, S. Mann, R.O.C. Oreffo, The potential of biomimesis in bone tissue engineering: lessons from the design and synthesis of invertebrate skeletons, *Bone*. 30 (2002) 810–815.
- [40] D. Puleo, Understanding and controlling the bone–implant interface, *Biomaterials*. 20 (1999)

2311-2321.

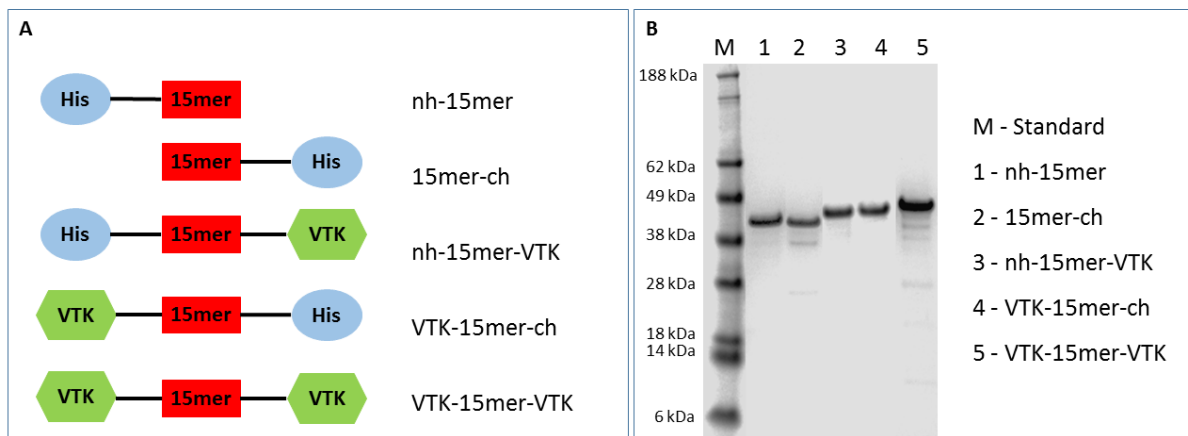


Fig. 1. Recombinant silk fusion protein design and production. (A) Schematic representation of fusion proteins design strategy; His-tag (blue circle) has been added to spider silk 15mer (red box) at N-terminal end of nh-15mer and nh-15mer-VTK constructs, and C-terminal end of 15mer-ch and VTK-15mer-ch constructs; VTK domain (green hexagon) has been added to the C-terminal of nh-15mer-VTK, N-terminal of VTK-15mer-ch and both N- and C-terminal of VTK-15mer-VTK. (B) SDS-page of purified nh-15mer (~40 kDa), 15mer-ch (~40 kDa), nh-15mer-VTK (~42 kDa), VTK-15mer-ch (~42 kDa) and VTK-15mer-VTK (~43 kDa), run on the 4% - 12% Bis-Tris acrylamide gel and stained with Simple Blue dye. Marker (M) sizes are indicated on the left.

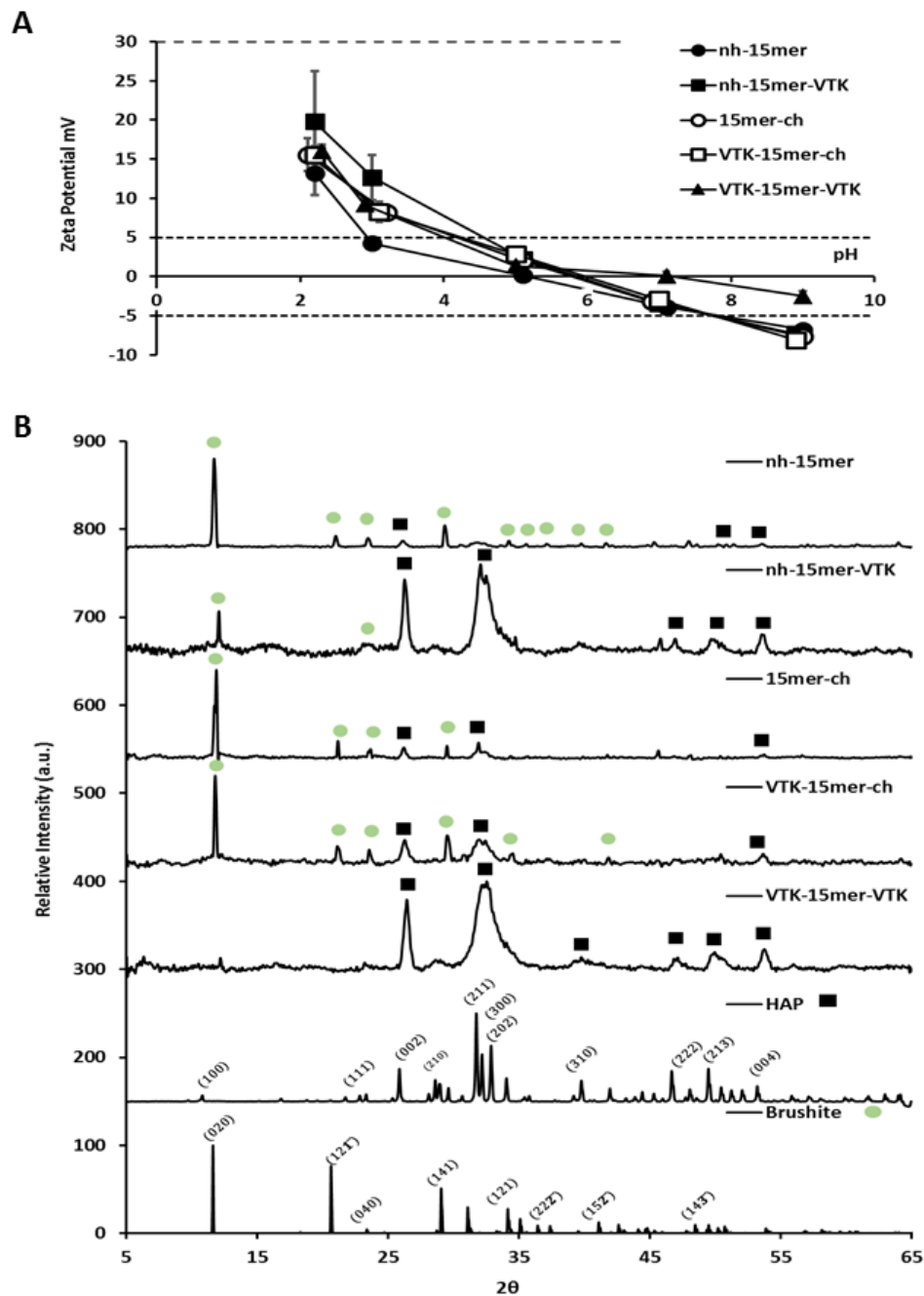


Fig. 2. Solution mineralization of silk proteins. (A) Zeta potential data over the pH range 2-9 for 1 mg/mL aqueous silk solutions, nh-15mer, nh-15mer-VTK, 15mer-ch, VTK-15mer-ch, and VTK-15mer-VTK, (n=5, p<0.05). (B) XRD data for the precipitates formed in the presence of each recombinant silk sample; nh-15mer, nh-15mer-VTK, 15mer-ch, VTK-15mer-ch and VTK-15mer-VTK.

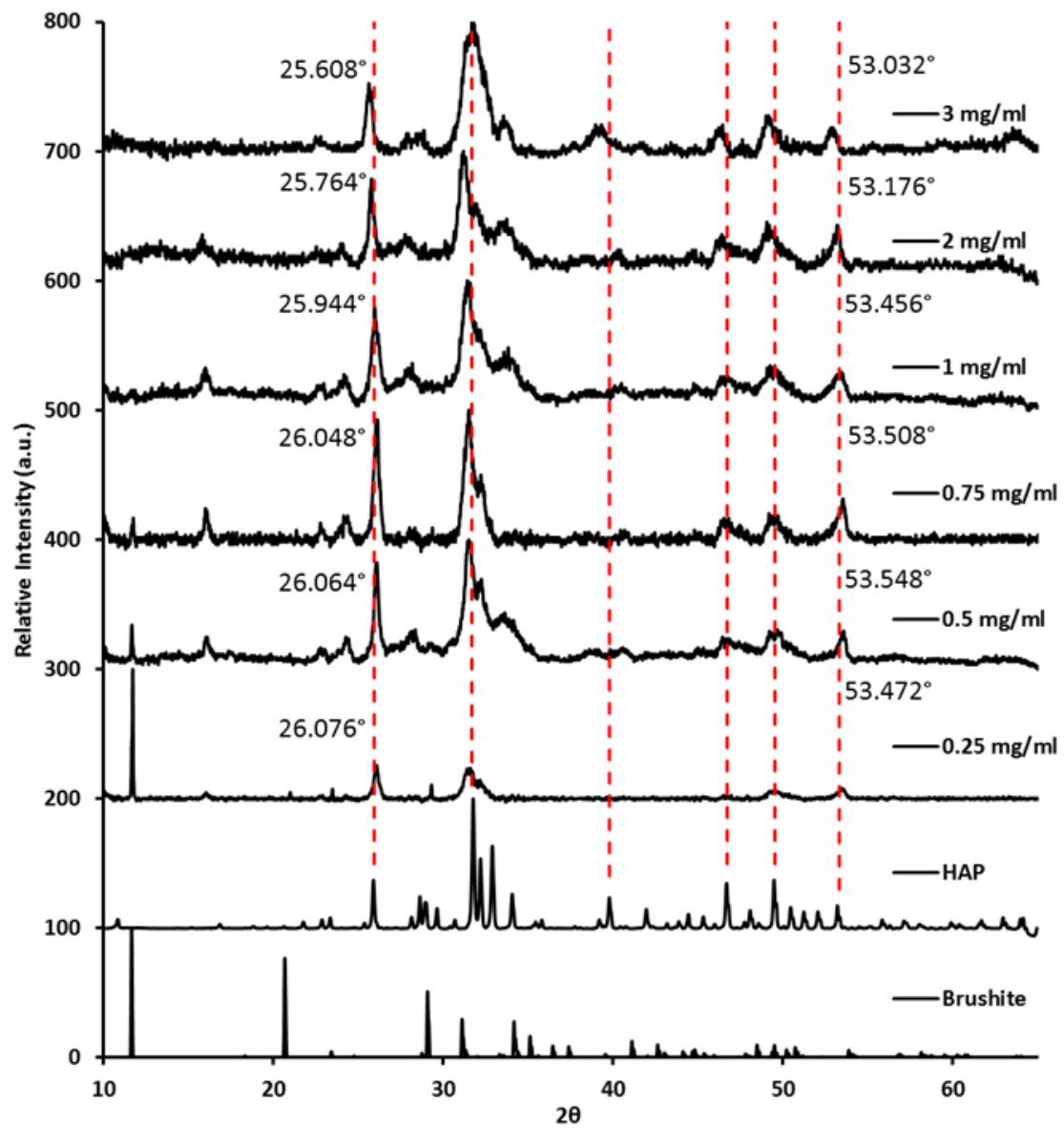


Fig. 3. Solution mineralization of silk proteins, XRD data for the precipitates formed in the presence of increasing concentration of VTK-15mer-VTK sample.

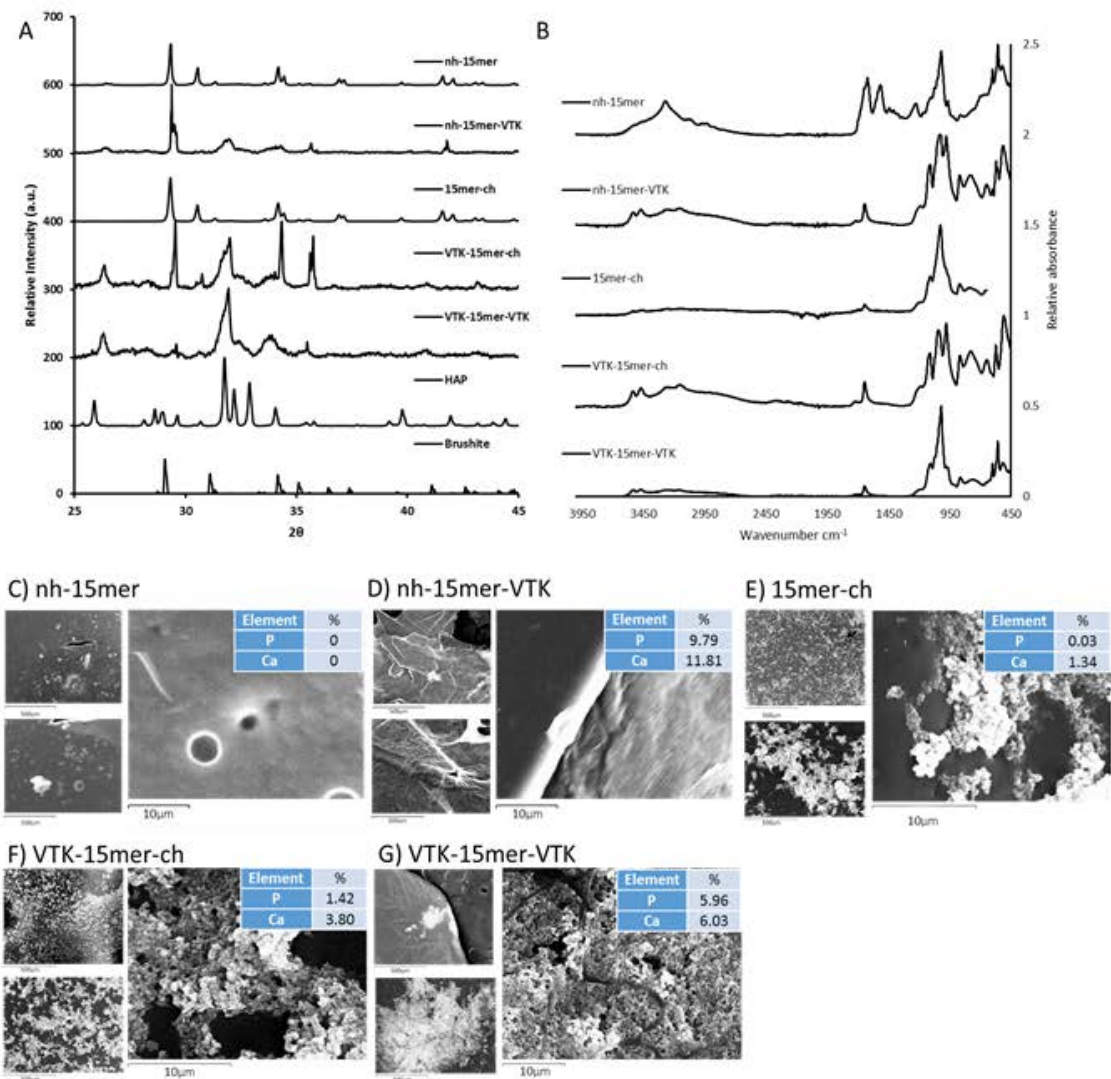


Fig. 4. Mineralization on recombinant silk films. (A) XRD patterns of the precipitates formed in the presence of: nh-15mer, nh-15mer-VTK, 15mer-ch, VTK-15mer-ch and VTK-15mer-VTK. (B) IR spectra for the precipitates produced. (C, D, E, F and G) SEM and EDX of the nh-15mer and nh-15mer-VTK,

15mer-ch, VTK-15mer-ch and VTK-15mer-VTK films respectively after 7 day mineralization. Scale bars are 500  $\mu\text{m}$ , 100  $\mu\text{m}$  and 10  $\mu\text{m}$ .

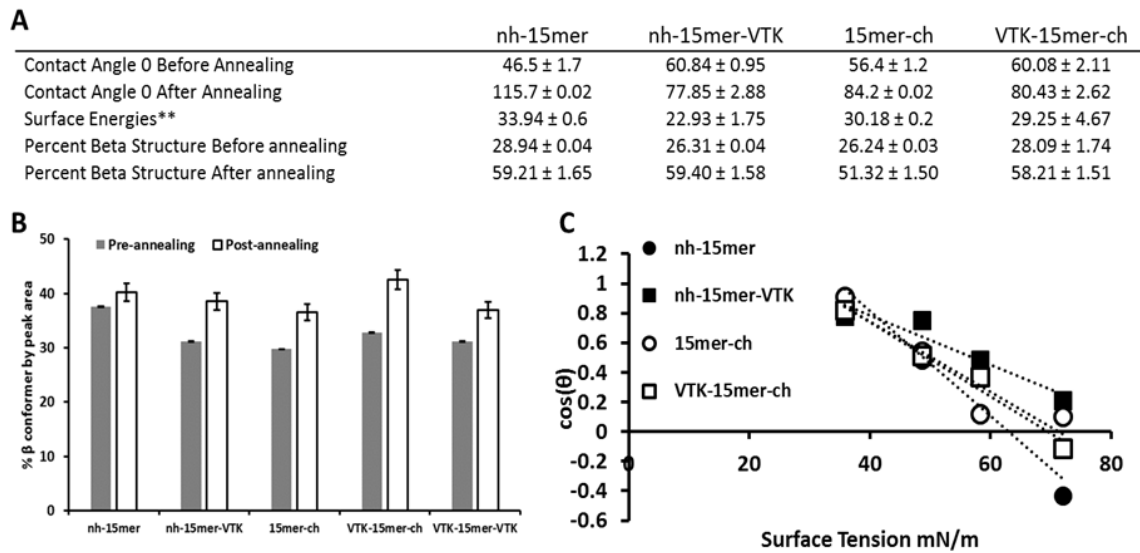
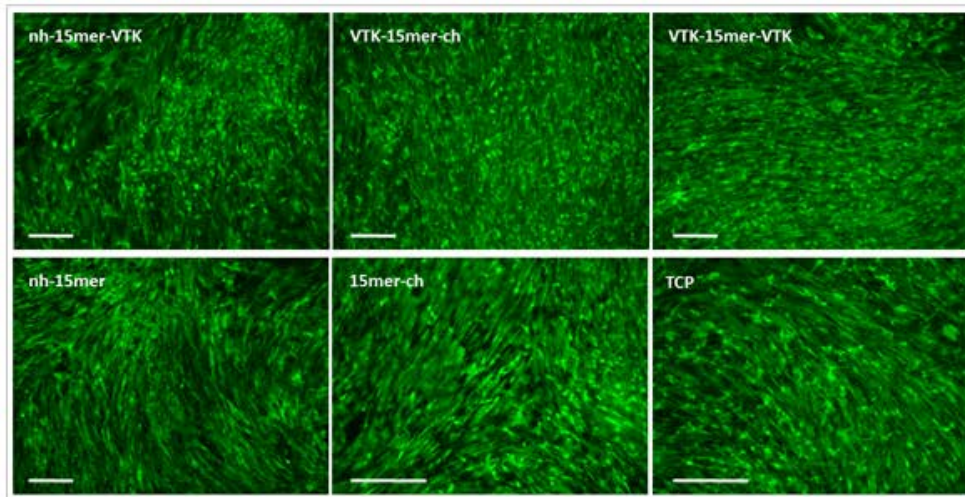


Fig. 5. Physical properties of chimeric silk films. (A) Table compiling the physical property data to observe any changes occurring from the addition of the VTK peptide. (B) Beta-sheet content of each silk film before and after annealing ( $n=5$ ,  $p<0.05$ ). (C) Zisman plots for each silk sample ( $n=5$ ,  $p<0.05$ ).

A



B

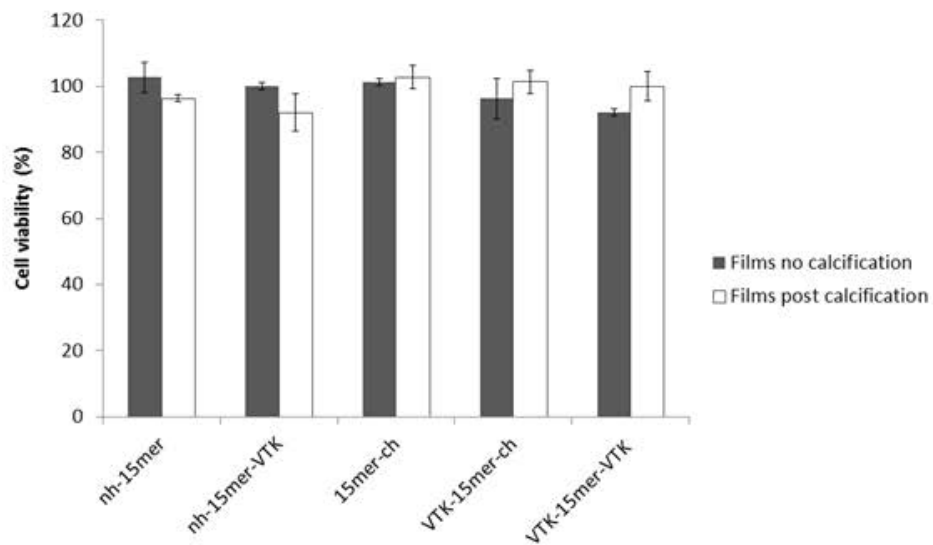
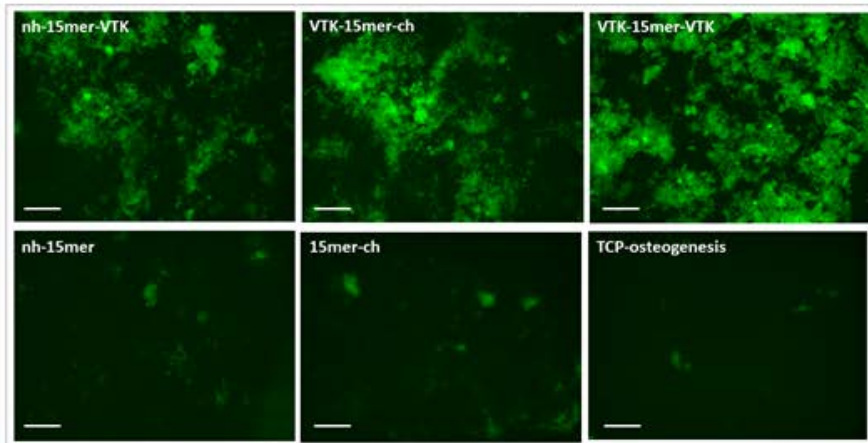


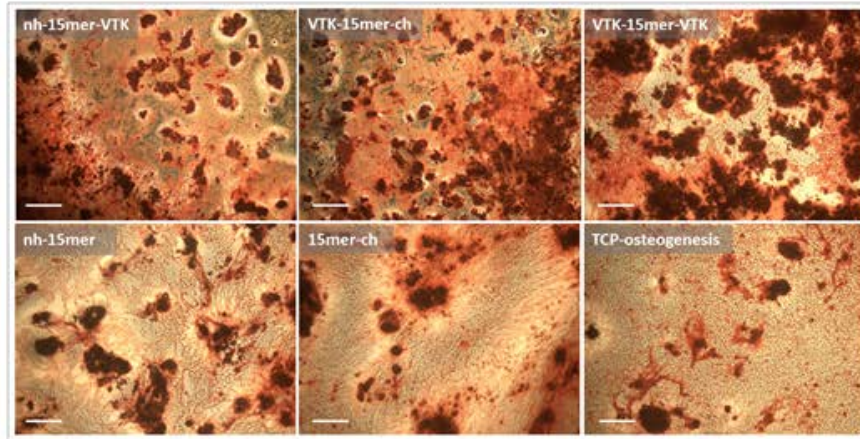
Fig. 6. Viability of human mesenchymal stem cell grown on recombinant silk and silk-VTK films before and after calcification. (A) Live (green) and dead (red) fluorescent staining was performed on hMSCs cells grown on calcified nh-15mer, nh-15mer-VTK, ch-15mer, ch-VTK-15mer, VTK-15mer-VTK and

tissue culture plate (TCP) two weeks post seeding. Scale bars are 200  $\mu\text{m}$ . (B) Comparison of cell proliferation on calcified (white bars) and non-calcified (black bars) recombinant silk films (nh-15mer, nh-15mer-VTK, 15mer-ch, VTK-15mer-ch, VTK-15mer-VTK) as determined by Alamar blue 2 weeks post-seeding. Data are represented as the average  $\pm$  standard deviation (n=3, \*p < 0.05).

A



B



C

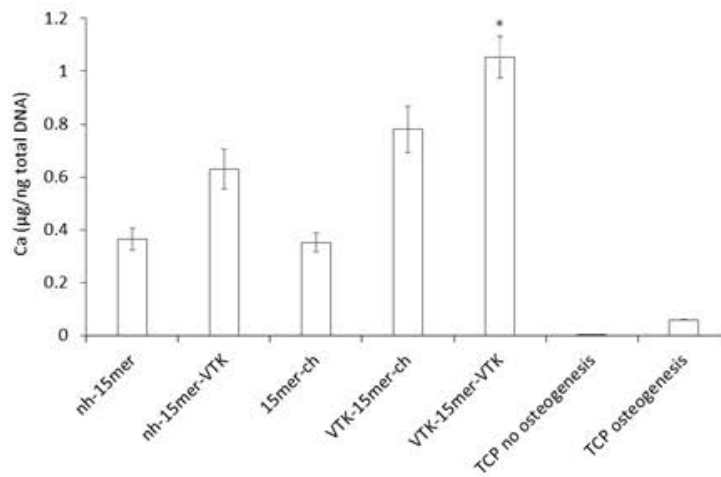
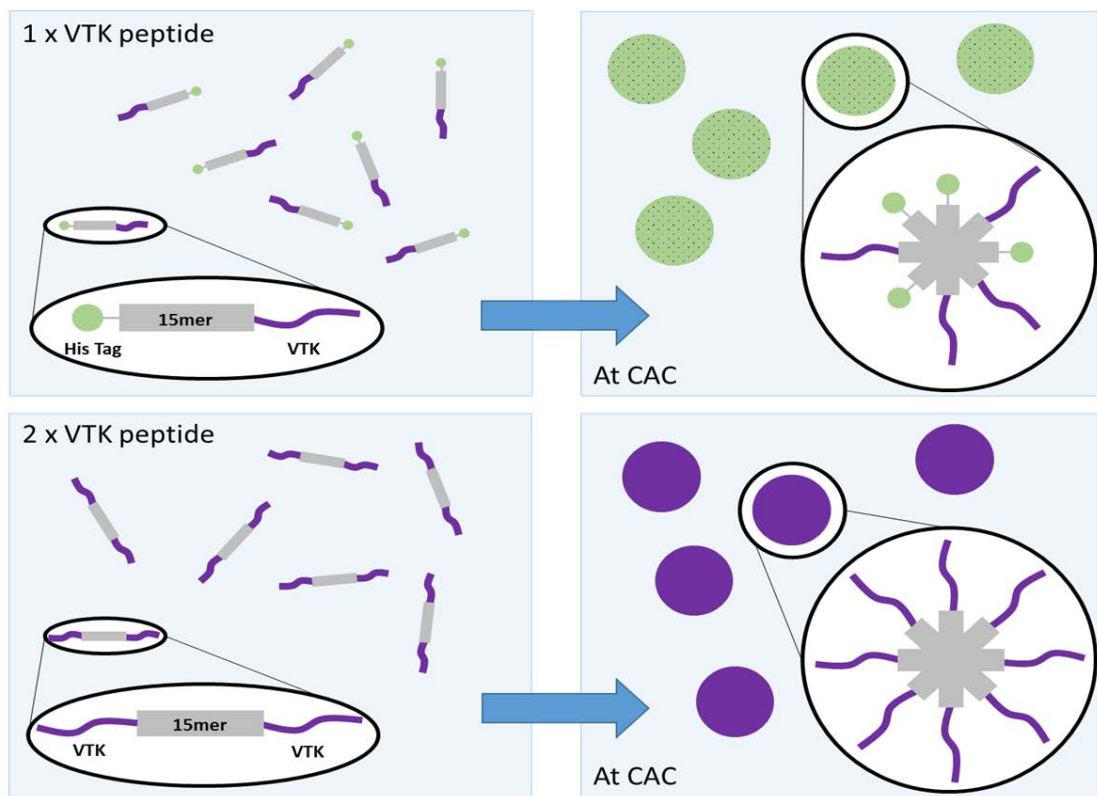


Fig. 7. Immunohistochemistry staining of bone sialoprotein produced by hMSC cells grown on recombinant silk and silk-VTK films (A) and calcium containing mineral deposition by differentiating human mesenchymal stem cell on the recombinant silk and silk-VTK films (B,C). (A) hMSC were grown

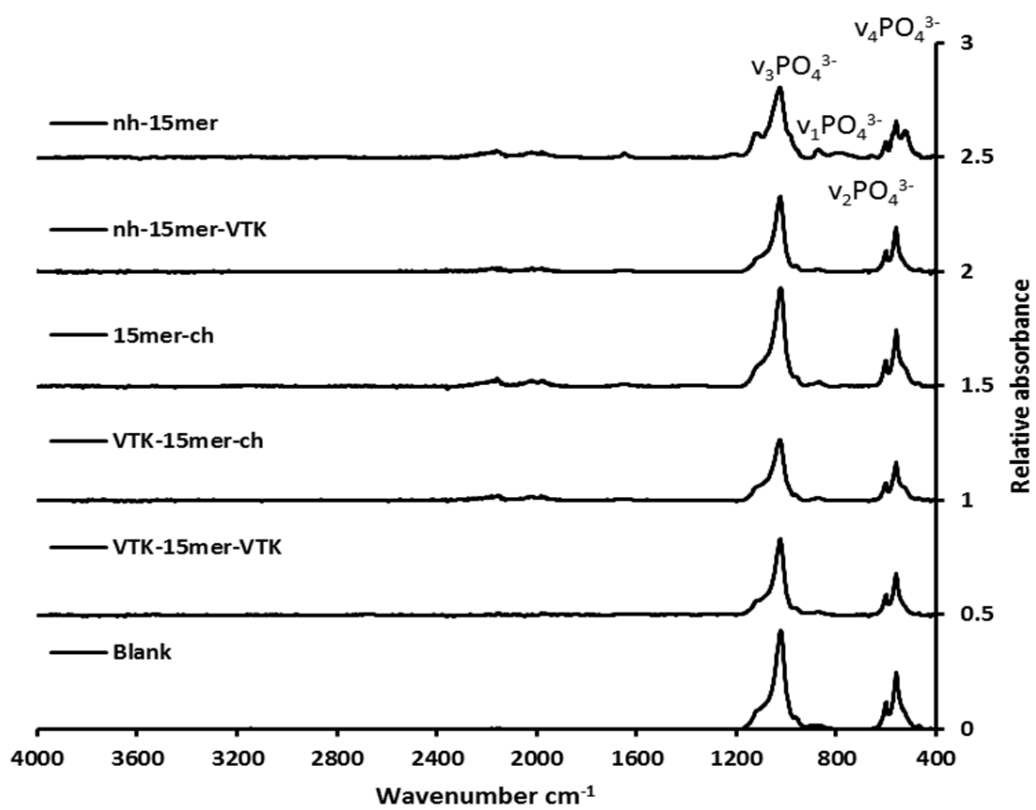
on recombinant nh-15mer, nh-15mer-VTK, 15mer-ch, VTK-15mer-ch and VTK-15mer-VTK films and TCP. Osteogenesis was induced and immunohistochemistry for bone sialoprotein performed 8 weeks post-seeding. Scale bars are 100  $\mu\text{m}$ . (B) Calcium containing mineral (red) staining by Alzarin Red S was performed on hMSCs cells grown on nh-15mer, nh-15mer-VTK, 15mer-ch, VTK-15mer-ch, VTK-15mer-VTK and TCP eight weeks post seeding. Scale bars are 300  $\mu\text{m}$ . (C) Quantitative analysis of calcium containing mineral deposition of hMSCs grown on recombinant slik-VTK constructs after 8 weeks in culture. Results for nh-15mer, nh-15mer-VTK, 15mer-ch, VTK-15mer-ch and VTK-15mer-VTK constructs and TCP no osteogenesis and TCP osteogenesis are shown. Data are represented as the average  $\pm$  standard deviation ( $n=3$ ,  $*p < 0.05$ ).

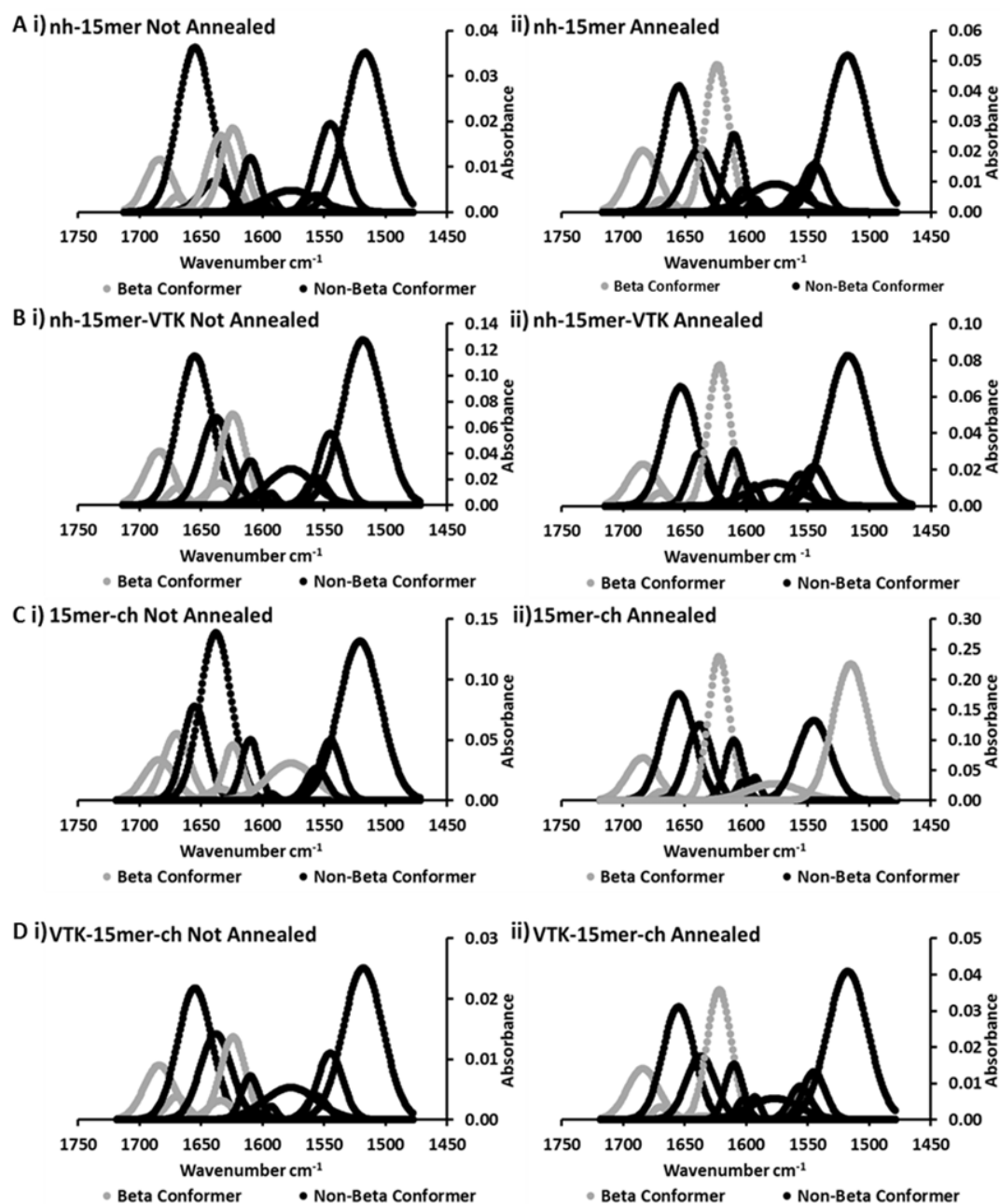


Scheme 1. Structural schematic of the assumed VTK peptide folding in solution when bound to the recombinant silk (A) and solution based mineralization comparing samples with one or two VTK peptides attached to the 15mer silk repeating unit (B). (A) When bound to the C termini of the silk, nh-15mer-VTK, the majority of the hydroxyl groups on the VTK peptide are at the opposite end to the

silk where there will be greater mobility and therefore solution interaction allowing heightened control over the precipitates formed. The opposite can be said of ch-15mer-VTK, where most hydroxyl groups will experience shielding and steric hinderance limiting solution interactions and control over mineralization. (B) With one terminus of the silk occupied with the HAP binding domain and the other the His Tag when protein aggregation occurs the two ends will organise in a non-uniform manner. When both ends of the silk are occupied by the VTK peptide non-uniform aggregation has no effect, as one HAP domain will always be exposed to the solution regardless of the orientation of the chimeric protein. CAC: critical aggregation concentration.

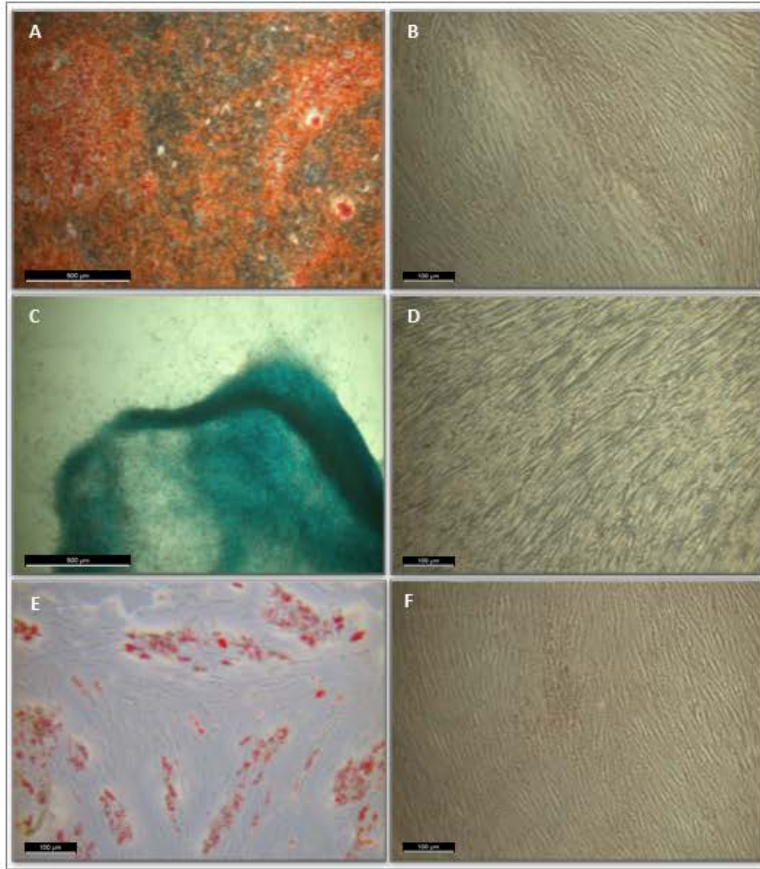
SI Figure 1. FTIR data collected of the precipitates formed in solution mineralisation in the presence of nh-15mer, nh-15mer-VTK, 15mer-ch, VTK-15mer-ch and VTK-15mer-VTK.





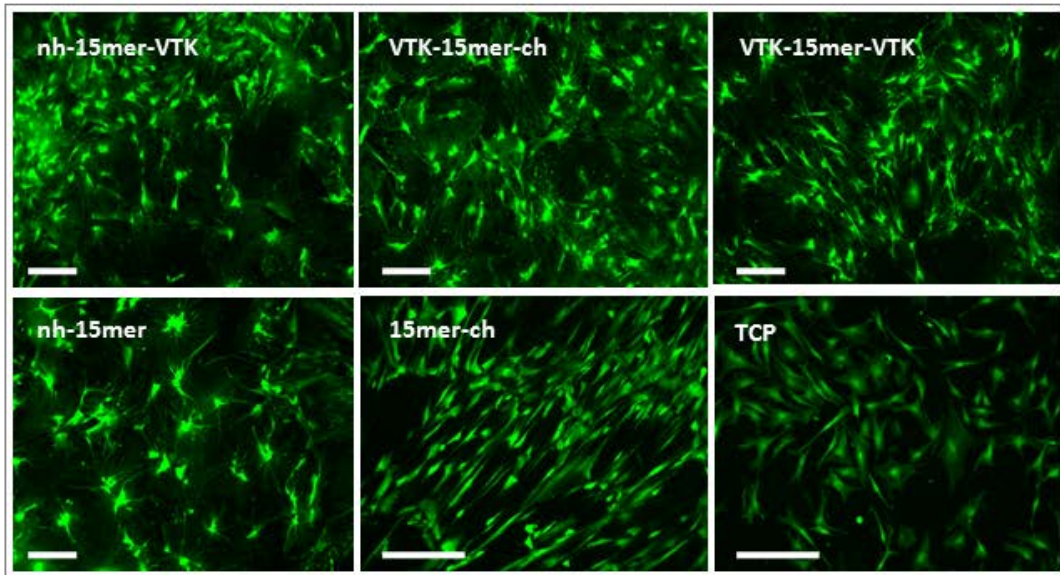
SI Figure 2. Example data: Comparison of recombinant silk films, nh-15mer, nh-15mer-VTK, 15mer-ch, VTK-15mer-ch, before and after the methanol annealing process with respect to the changes in protein secondary structure.



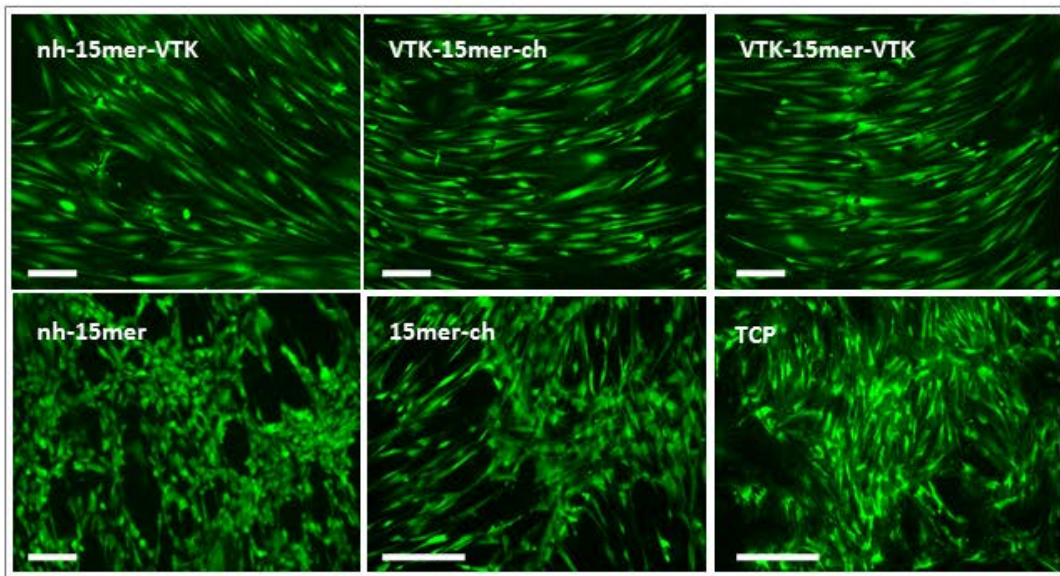


SI Figure 3. Characterization of hMSC potential for differentiation. (A, B) Osteogenic differentiation of P2 hMSC in pellets cultured either in osteogenic medium (A) or in control medium (B). Scale bar 500  $\mu\text{m}$  (C), 100  $\mu\text{m}$  (D). Stain: Alizarin Red S (mineralized bone matrix is shown in red). (C,D) Chondrogenic differentiation of P2 hMSC in pellets cultured either in chondrogenic medium (C) or in control medium (C). Scale bar 500  $\mu\text{m}$  (C), 100  $\mu\text{m}$  (C). Stain: Alcian Blue (cartilaginous glycosaminoglycan, GAG, is shown in blue). (E,F) Adipogenic differentiation of P2 hMSC in pellets cultured either in adipogenic medium (E) or in control medium (F). Scale bar 100  $\mu\text{m}$  (E), 100  $\mu\text{m}$  (F). Stain: Oil Red O (lipid droplets are shown in red).

A



B

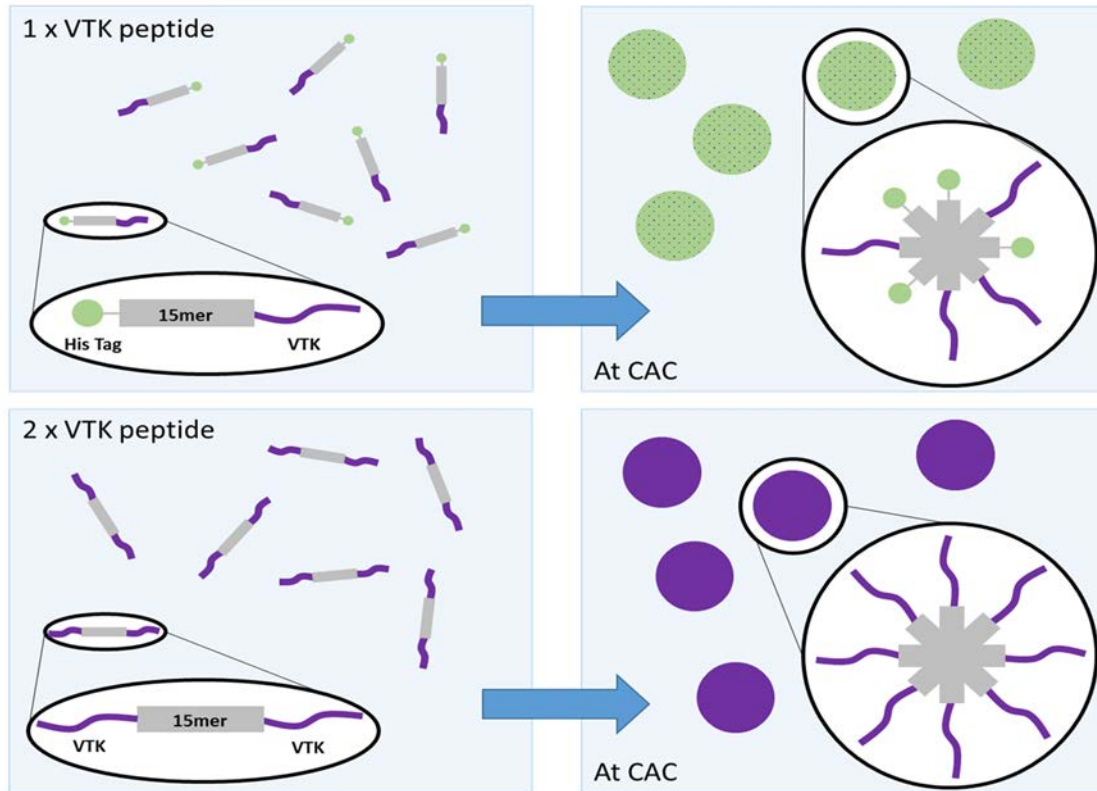


SI Figure 4. Viability of human mesenchymal stem cell grown on recombinant silk and silk-VTK films.

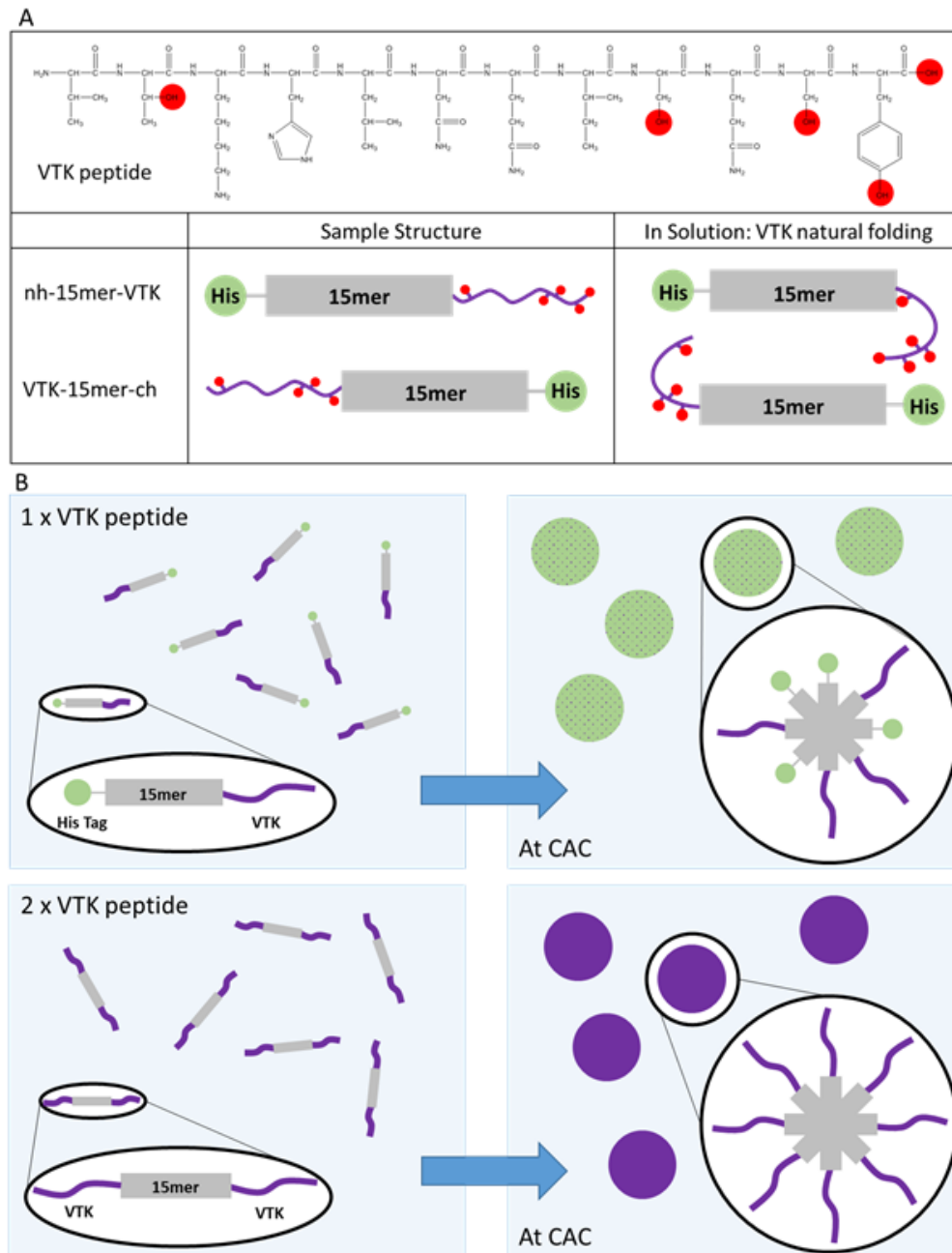
(A,B) Live (green) and dead (red) fluorescent staining was performed on hMSCs cells grown on calcified

nh-15mer, nh-15mer-VTK, ch-15mer, ch-VTK-15mer, VTK-15mer-VTK and tissue culture plate (TCP) 3

(A) and 7 days post seeding (B). Scale bars are 200  $\mu\text{m}$ .



G



Graphical Abstract